Analyzing the Complex Impedances of All LHC Main Dipole Magnets

M. Janitschke, M. Bednarek, J. Ludwin, E. Ravaioli, A.P. Verweij, and U. van Rienen

***Abstract*—Measuring a superconducting magnet's complex impedance as a function of the frequency is a promising diagnostic tool to investigate its electrical integrity and the potential presence of electrical nonconformities. Such transfer function measurements (TFM) were performed for the first time on a large number of magnets in the Large Hadron Collider (LHC). During this measurement campaign, the impedances of all 1232 superconducting main dipoles installed in the LHC were measured at cold in the frequency range from 1 Hz to 100 kHz. This letter presents the measurement set-up and provides a comparative data analysis of all complex impedance measurements. Distinct groups of magnets showing similar behavior are analyzed, and frequency ranges showing significant impedance variations are identified. Variations in TFM are shown to be correlated to individual features of each magnet, such as manufacturing tolerances in the magnets' beam screens, different materials used in their coil-protection sheets, and variations in the critical current of their superconductors. Moreover, measurements are compared to the simulation results obtained by a recently developed and validated lumped-element network model and show good agreement. Finally, a few magnets are identified as outliers as their measured impedances deviate significantly from the impedances of the other magnets and differ from the simulated values.**

***Index Terms*—Accelerator magnets, ac loss, data analysis, fault diagnostics, impedance, machine learning, superconducting coil.**

I. Introduction

SUPERCONDUCTING magnets in particle accelerators are subject to various strong disturbances, such as high voltages, thermal gradients, radiation, or mechanical forces, over their lifetime. Ensuring their reliable operations is paramount for the operation of the accelerator, as any failure can cause costly downtime and repairs. Detecting failures or their precursors at an early stage can significantly increase the availability and reliability of the entire machine.

Received 21 September 2024; revised 14 January 2025; accepted 26 January 2025. Date of publication 30 January 2025; date of current version 18 February 2025. This work was supported by the Wolfgang Gentner Programme of the German Federal Ministry of Education and Research under Grant 13E18CHA. *(Corresponding author: M. Janitschke.)*

M. Janitschke is with CERN, CH, 01631 Geneve, Switzerland, and also with the University of Rostock, DE, 180515 Rostock, Germany (e-mail: marvin.janitschke@cern.ch).

M. Bednarek, E. Ravaioli, and A.P. Verweij are with CERN, CH, 01631 Geneve, Switzerland.

J. Ludwin is with CERN, CH, 01631 Geneve, Switzerland, and also with IFJ PAN, PL, 31-342 Krakow, Poland.

U. van Rienen is with the University of Rostock, DE, 180515 Rostock, Germany.

Color versions of one or more figures in this article are available at https://doi.org/10.1109/TASC.2025.3536437.

Digital Object Identifier 10.1109/TASC.2025.3536437

Among many possible failures, insulation failures in the coil of a superconducting magnet are of particular concern, as their precursors can be very challenging to detect once the magnet is installed in the accelerator. Impedance measurements are a promising diagnostic tool used to assess the integrity of superconducting magnets, as they provide valuable insights into the electrodynamic characteristics of the magnet. Unexplained changes in impedance can indicate the presence of a failure or its precursor [1], [2], [3].

For the first time, such impedance measurements were performed on a large number of magnets in the Large Hadron Collider (LHC) during the yearly technical stop at the beginning of 2024. During this transfer function measurement (TFM) campaign, the impedance of all 1232 main dipoles installed in the LHC was measured in a frequency range of 1 Hz to 100 kHz. Systematically measuring the impedances of the superconducting main dipoles can establish the baseline impedance characteristics. Comparing future measurements to this baseline will immediately indicate impedance changes.

To effectively use impedance measurements for failure diagnostics, it is essential to determine whether impedance variations are due to factors like manufacturing tolerances or if they require further investigation. This contribution will present a comprehensive analysis of the measurements. Frequency ranges with significant impedance variations between the magnets are analyzed. Distinct groups of magnets showing similar impedances within these ranges are identified. The existence of these groups is related to different materials used for the coil-protection sheets (CPS), different cable manufacturers, and manufacturing tolerances in the beam-screens (BS). As a result, each main dipole in the LHC can be assigned to one of the identified groups, each with a comparably small standard deviation. This facilitates the identification of outliers among the magnets.

In addition, simulations of the main dipole impedances can enhance the understanding of measurements and assist in predicting and analyzing failures, such as insulation issues. This article's final part will discuss the applicability and scope of a recently developed and validated physics-driven lumped element model, which incorporates several nonlinear electrodynamic coupling effects [4], [5].

II. Measurement Set-Up

Each main dipole magnet consists of two apertures electrically connected in series, with coils using two different Nb-Ti Rutherford cables for the outer and inner layers. The magnet has a magnetic length of $l_{\mathrm{mag}} = 14.3$ m and generates a dipole

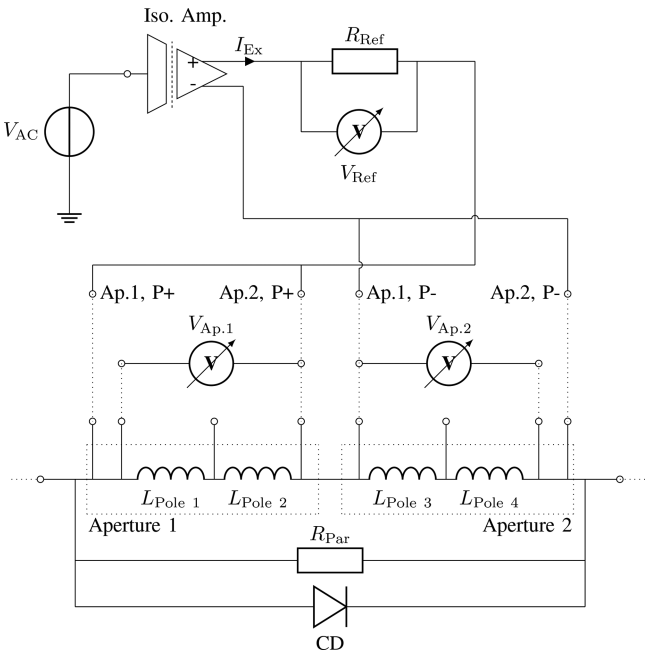

Fig. 1. Schematic showing the measurement set-up for the two individual apertures of one main dipole in the LHC tunnel. Only one aperture is powered (P+, P−) and measured in 4-wire mode at a time.

field of $B_{\mathrm{Nom}} = 8.3$ T at nominal current $I_{\mathrm{Nom}} = 11.85$ kA and operating temperature $T_{\mathrm{Nom}} = 1.9$ K. The superconducting coils are covered by CPS before collaring and contain a BS tube within their bore. Each dipole has a cold diode and a resistor $R_{\mathrm{Par}} = 100\ \Omega$ in parallel [6], [7]. One main dipole circuit consists of two branches, each with 77 magnets in series. The measurements were performed at T_{Nom}, and the branches were not connected and were left floating.

The set-up for the measurements of the individual main dipole apertures is shown in Fig. 1. The impedance was measured with a PowerTek GP102 gain/phase analyzer that excites the magnet with a sinusoidal voltage of amplitude $V_{\mathrm{AC}} = 10$ V. The input current is deduced by measuring the voltage across a reference resistor of $R_{\mathrm{Ref}} = 25\ \Omega$ [8], limiting the maximum current to $I_{\mathrm{Max,Ex.}} = 0.4$ A at low frequencies. The maximum field change within the aperture's center is limited to 0.175 mT. To limit the parasitic effects of the chain and noise, the generator's output signal is separated from the ground with an isolation amplifier. Only magnets on the extremities of the branches show slightly different behavior at higher frequencies with respect to the other main dipoles. The measurements were performed in 4-wire mode, using different voltage taps to excite the magnet and to measure the voltage across the aperture. to exclude the influence of voltage tap resistance.

The complex impedance is given by $\mathbf{Z} = \mathbf{V}_{\mathrm{Ap}}/\mathbf{V}_{\mathrm{Ref}} \cdot R_{\mathrm{Ref}}\,[\Omega]$ with additional compensation of internal impedances of the measurement system. The impedance was measured for frequencies ranging from 1 Hz to 100 kHz with 24 points per decade.

In total, four identical systems were used during the measurement campaign. The systems were calibrated and compared on a reference magnet in the LHC. The maximum impedance error introduced by the different systems and over time is below 0.3% for frequencies up to 10 kHz and below 3% for higher frequencies.

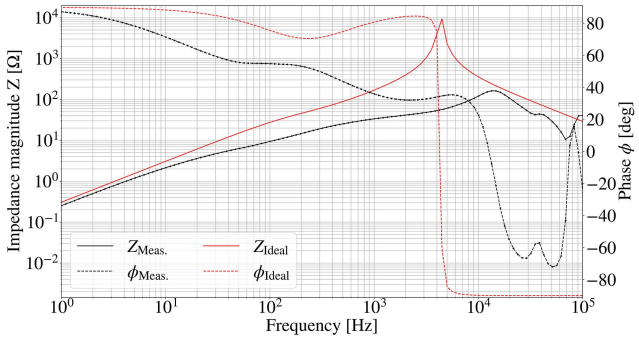

Fig. 2. Measured impedance magnitude and phase shift of one LHC main dipole aperture and an ideal LC-representation ($L = 49$ mH, $C = 160$ nF), both with a parallel resistance $R_{\mathrm{Par}} = 100\ \Omega$.

III. Measurement Results

An example of the measured impedance of one LHC main dipole aperture is shown in Fig. 2. The measurement is compared to an ideal *LC* representation of a superconducting magnet. One can observe that the measurement deviates at all frequencies from the ideal representation due to dynamic coupling effects within the magnet [5].

A set of in total more than 40 features for each aperture was gathered to evaluate this grouping and its reasons. The features contain information and measurements of the magnets, such as the cable manufacturers of each layer, the measured average magnetization M_{Avg} [mT], and the average residual-resistivity ratio RRR_{Avg} [−] of the strands copper. Moreover, manufacturing information is included, such as the material used for the CPS or the surface resistances of the apertures BS $R_{\mathrm{BS,surface}}$ [Ω].

The impedances were clustered into distinct groups using the k-means clustering algorithm and a combination of the elbow and silhouette methods [9] to identify the optimal number of groups. The number of groups as a function of the frequency can be seen in Fig. 3. The Fisher ratio (F-ratio) was used to select the most important features, which describes the separability of features. It is defined as the ratio of the covariances of a feature between the clusters and the covariances of a feature within each cluster, as follows [10]:

$$F = \frac{\frac{1}{K-1}\sum_{l=1}^{K}\left(\overline{x}_l - \frac{1}{K}\sum_{j=1}^{K}\overline{x}_j\right)^2}{\frac{1}{K}\sum_{j=1}^{K}\left(\frac{1}{n_j-1}\sum_{i=1}^{n_j}(x_{ij}-\overline{x}_j)^2\right)} \quad [-] \qquad (1)$$

with K [−] the total number of clusters, n_j [−] the number of elements in cluster j with mean $\overline{x}_j$, and x_{ij} the ith feature within the cluster j. The F-ratios are shown in Fig. 3. A random-forest-classifier (RFC) [11] was used to test classification accuracy, only utilizing the most important features as inputs. The average prediction accuracy over a K-fold-cross-validation with ten folds is shown in Fig. 3. As expected, the prediction accuracy of the classifier is higher when the F-ratio of the feature is larger.

Fig. 4 presents the measurement results for all 2464 apertures. In total, 24 groups are identified as the combination of two

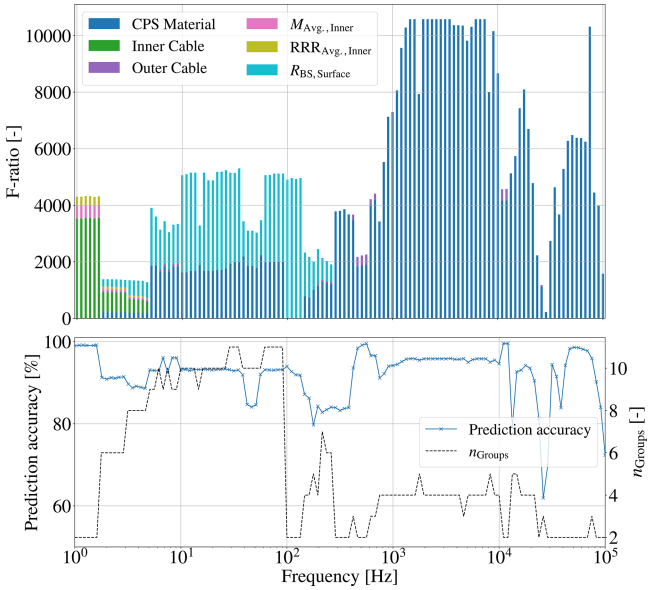

Fig. 3. F-ratios of the features for all frequencies, where the complex impedances of all apertures were clustered into n_{Groups} and the prediction accuracy of an RFC using only the identified features as input. Small F-ratios are neglected.

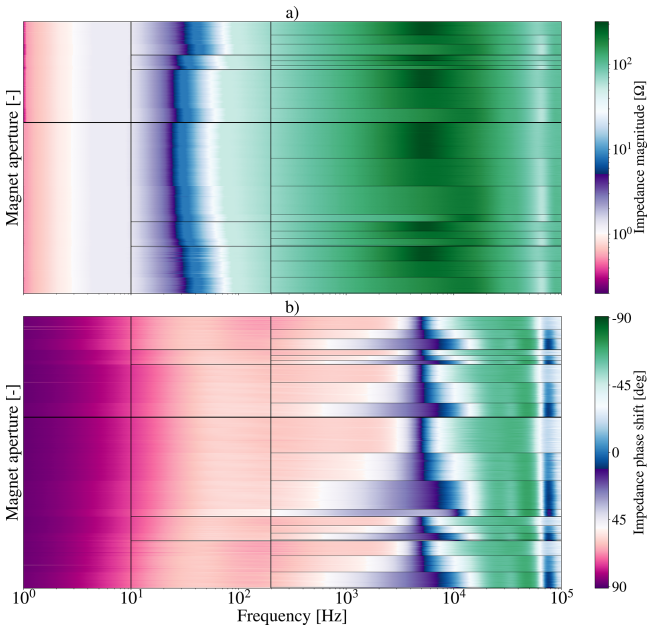

Fig. 4. Measurement results of (a) impedance magnitude and (b) impedance phase shift of all 2464 LHC main dipole apertures.

groups, visible at low frequencies around 1 Hz, three at intermediate frequencies ranging from 10 to 300 Hz, and four at higher frequencies. The following subsections discuss the grouping and their reasons in more detail.

A. Low Frequency Range up to 10 Hz

The impedances at low frequencies are defined by the inductive behavior of the magnet and all coupling currents with large

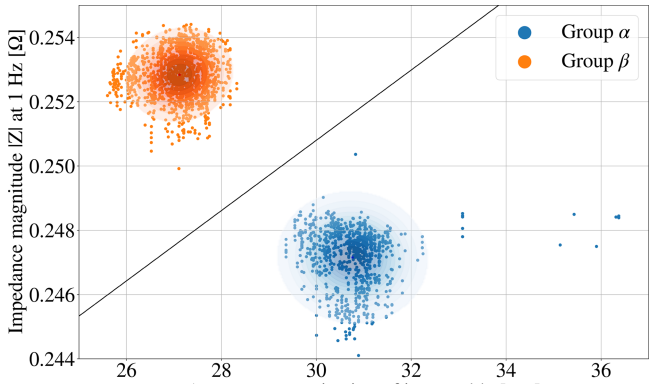

Fig. 5. Measured impedance magnitude of the LHC main dipole apertures at 1 Hz versus the measured average magnetization of the inner cable. Clusters are separated with the linear discriminant (solid line), and contours indicate each cluster's centered, normal distribution up to 3σ.

time constants [4], [5]. As shown in Fig. 3, the inner cable's manufacturer and measured average magnetization, both strongly correlated [12], could be identified for grouping at low frequencies. Fig. 5 shows the inner cable's average magnetization versus the measured impedance at 1 Hz. One can identify two distinct groups, α and β, with an inverse relation between magnetization and impedance magnitude. The larger the magnetization of the inner cable, the larger the effect of the persistent currents on the differential inductance of the magnet, and hence a smaller impedance [4], [5], [13]. However, some magnet apertures with a significantly higher measured magnetization do not show a smaller impedance. As can also be seen in Fig. 3, other features of the inner cable also impact the impedance, which will be investigated more closely in the future.

B. High-Frequency Range Between 300 Hz and 10 Khz

At higher frequencies, before the resonance peak of the transfer function, the impedance is mainly governed by eddy currents in other metallic magnet components [4]. Fig. 3 indicates a separation of all 2464 apertures into four groups due to the material used for their CPS. The resistivities of these materials are significantly different and range between 60 n Ω m up to about 600 n Ω m and, therefore, the eddy currents that develop within the CPS [4].

In Fig. 6, the average impedance magnitude μ within all four groups, the uncertainty spread of three times the standard deviation σ, and the coefficient of variation σ/μ are shown. The variation of the impedance magnitude due to the different materials in the CPS can reach up to a factor of five at a frequency of about 5 kHz. However, after the grouping, one can notice that the uncertainty spread around each group's average becomes very narrow.

C. Medium Frequency Range Between 10 and 300 Hz

Differences in the eddy currents can explain the clustering in the medium frequency range between 10 and 300 Hz developed in the copper layer of the apertures BS [4], [14], [15]. The BS is a copper-coated stainless steel tube inside the

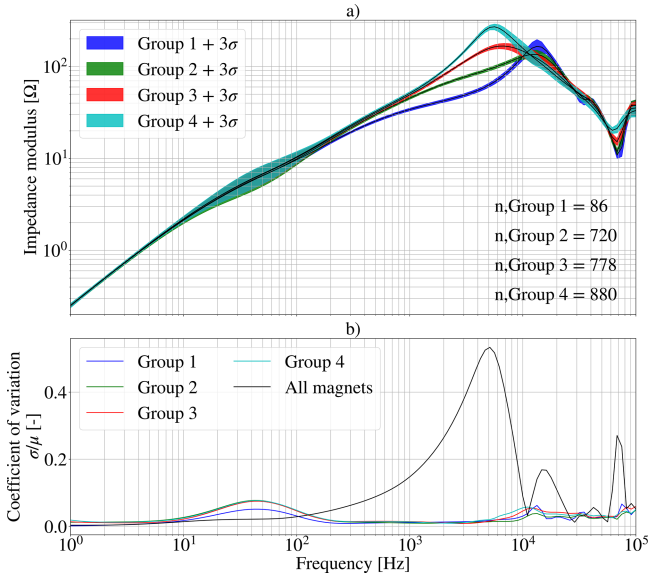

Fig. 6. (a) Measured average impedance magnitude within all four identified groups, indicating the spread of impedances within a group with a 3σ range. (b) Coefficient of variation σ/μ between the groups and among all magnets. The numbers of apertures within each group are denoted in Fig. 6(a).

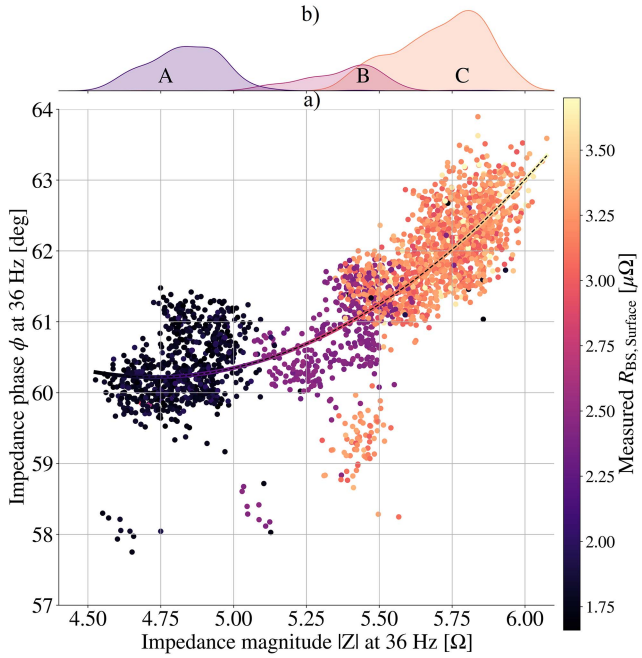

Fig. 7. (a) Measured impedance magnitude versus phase shift at 36 Hz of all LHC main dipole apertures, and (b) the distribution of measured surface resistances of the apertures BS. The centerline shows the correlation between phase and impedance and the prediction of surface resistance using ordinary least squares [10].

magnets' aperture [7]. Due to manufacturing tolerances, the purity and thickness of the copper coating can vary significantly between the different batches produced and installed in the LHC [16]. A closer analysis showed a strong correlation between the measured impedance of the aperture and the measured surface resistance of this copper coating, as shown in Fig. 7 at a frequency of 36 Hz. A larger surface resistance correlates to a larger impedance magnitude. Copper coatings with a higher resistivity cause less eddy currents, reducing the magnets' impedance. Moreover, one can notice a separation into three groups: A, B, and C, resulting in combination with the CPS groups in a total of 12 groups. The maximum spread of variation in Fig. 6 of about 70% at frequencies between 10 and 300 Hz can be further reduced below 10% by including these groups.

IV. Comparison to Simulations

A recently developed and validated physics-driven lumped-element network model was used to simulate the impedances of all 2464 LHC main dipole apertures [4]. This model incorporates nonlinear dynamic coupling effects, including persistent currents, interfilament and interstrand coupling currents, and eddy currents in the strands' copper [17], [18] and metallic components. Each aperture model includes individual as-built parameters of the BS and CPS. The difference between the measurements and the simulations can be seen in Fig. 8. Even though the impedance changes by orders of magnitude, the difference between the measurements and the simulations generally ranges below 10% for frequencies below 1 kHz, with an average error of 3.8% and 6.7% for impedance magnitude and phase shift, respectively. For frequencies up to 10 kHz, the agreement in the impedance magnitude is still very good, within 4% . However,

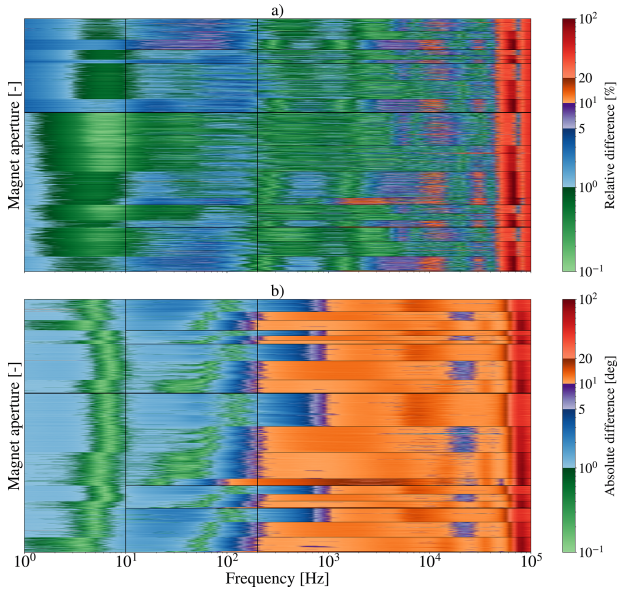

Fig. 8. (a) Relative difference of the impedance magnitude $|Z|$ and (b) absolute difference of the impedance phase shift ϕ between simulations and measurements.

due to differences at which the resonance peaks are simulated, the error in the phase shift increases to 38% .

The simulations show very good agreement with the measurements. Future simulations could also include more available information about the individual magnets, such as the measured magnetization or RRR. This could, for example, improve the

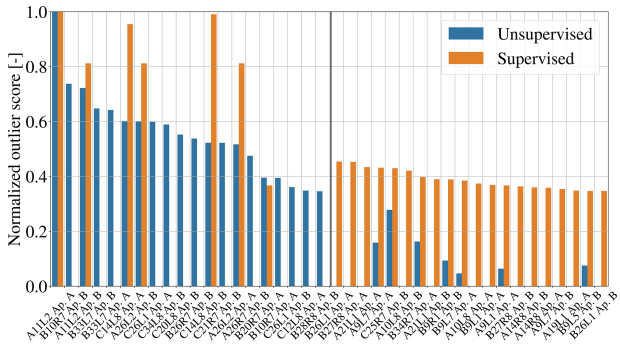

Fig. 9. In total, 20 LHC main dipole apertures (A, B) which were detected as the most significant outliers using unsupervised and supervised outlier detection. The outlier scores for each method were standardized to be within 0 and 1.

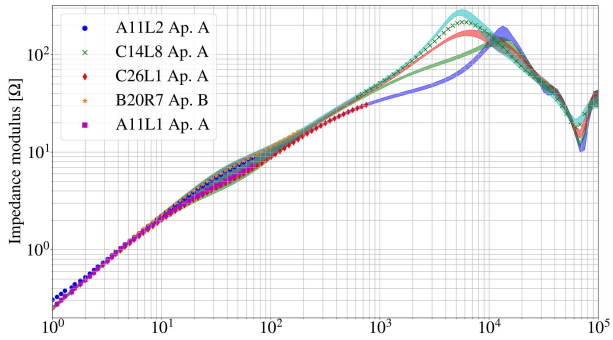

Fig. 10. Five selected LHC main dipole apertures that were classified to be among the most significant outliers by the unsupervised algorithms. Shaded areas indicate the four identified CPS groups, as shown in Fig. 6. Impedance magnitudes of the outliers are only highlighted in the frequency range, where they are considered an outlier.

accuracy of the simulations of group α (compare to upper blocks in Fig. 8). As such, the simulations can be used for two purposes. First, to enhance the understanding of the impedances. A direct mapping of physical parameters to the model makes it possible to explore the effect of different coupling effects directly onto the magnets' impedance. Second, the model could simulate the impact of faults, such as interturn shorts on the impedance and assess the magnets' performance.

V. Outlier Detection

The impedance measurements of the main dipole apertures were analyzed for outliers using a two-fold approach. First, a supervised algorithm based on the standard score identified outliers when the measured impedance magnitude deviated by more than 3σ from their group average at a given frequency. This algorithm detected 50 outliers: six deviated by more than 5σ and five by more than 4σ. Four of the six exceeding 5σ were known nonconformities, and two were from a unique refurbished magnet with a different CPS material. The remaining 44 outliers will be further investigated.

Second, outliers were found with an unsupervised analysis. This analysis combined multiple unsupervised outlier detection methods, such as density-based methods (Local Outlier Factor), cluster-based methods (K-nearest neighbors), and bagging methods (random forest) to increase the robustness of the overall algorithm [19], [20]. Each method was applied to the same dataset multiple times with different initializations, and the overall average was used to make the outlier decision. Moreover, this approach was also applied to the relationship between the impedance- and phase-derivatives over the frequency. The unsupervised approach detected 86 outliers, with 29 overlapping with those identified by the supervised method, including those deviating by more than 5σ. The 20 outliers with the highest outlier scores are shown for the two approaches in Fig. 9.

The impedance magnitudes of selected outliers among the highest outlier scores are shown in Fig. 10. The first outlier aperture shows a significantly larger impedance at low frequencies. This is due to a different wiring connection on the voltage tap level and hence includes parts of the resistances of the measurement cables. Another aperture, from magnet C14L8, shows a different behavior at frequencies above 300 Hz. Based on prior knowledge, an investigation of this magnet showed that it is a refurbished magnet, in which another, different material was used for the CPS. For the remaining three magnet apertures that are shown in Fig. 10 no explanation is known yet. All three are classified as outliers from low frequencies up to 300 Hz. These magnets and the remaining magnets from both detection algorithms will be investigated more closely. In this analysis, previously identified outlier magnets in [21] were not identified as outliers.

VI. Conclusion and Outlook

This article presents the first comprehensive study of the impedances of all LHC main dipoles measured during the TFM campaign. The analysis identified 24 distinct impedance groups and behaviors correlating with magnet data: at low frequencies, the inner cable magnetization; at intermediate frequencies, the BS surface resistance; and at high frequencies, the CPS materials. Variations in coupling currents were found to be not significant between the magnets. A set of outliers was found, with known nonconformities or other known reasons for their deviation. The remaining outliers will be investigated more closely in the future.

With a reproducibility error of less than 0.3% , future measurements can be directly compared to the acquired impedance data to detect changes and identify potential fault precursors. Comparing the impedance measurements to models of all 2464 main dipole apertures showed a very good agreement, with an average error in the magnitude below 5% up to 10 kHz. The validated models can be used to investigate the impact of electrical nonconformities on the magnet performance and highlight how specific faults or precursors would manifest in the data.

Acknowledgment

The authors would like to thank all colleagues at IFJ PAN and CERN involved during the YETS 2023/2024, in particular G. D'Angelo.

REFERENCES

[1] H. Ehmler et al., "Comparative analysis of impulse and impedance tests to detect short circuits within the W7-X magnets," *IEEE Trans. Appl. Supercond.*, vol. 16, no. 2, pp. 767–770, Jun. 2006.

[2] H. Ehmler, I. R. Dixon, T. A. Painter, and J. A. Powell, "Electrical AC tests on CICC coil for series-connected hybrid magnet," *IEEE Trans. Appl. Supercond.*, vol. 22, no. 3, pp. 9002204–9002204, Jun. 2012.

[3] A. Foussat, L. Grand-Clement, D. Smekens, F. O. Pincot, L. Bortot, and F. Savary, "Frequency-domain diagnosis methods for quality assessment of Nb_3Sn coil insulation systems and impedance measurement," *IEEE Trans. Appl. Supercond.*, vol. 28, no. 3, Apr. 2018, Art. no. 4003505.

[4] M. Janitschke, M. Bednarek, E. Ravaioli, A. P. Verweij, G. Willering, and U. van Rienen, "Physics-driven lumped-element modelling for impedance simulations of superconducting accelerator magnets," *Supercond. Sci. Technol.*, vol. 38, no. 1, Dec. 2024, Art. no. 015013, doi: 10.1088/1361-6668/ad9ad8.

[5] M. Janitschke et al., "Validating the physics-driven lumped-element model of the LHC main dipole magnet," *IEEE Trans. Appl. Supercond.*, vol. 34, no. 5, Aug. 2024, Art. no. 4004405.

[6] L. Rossi, "The LHC main dipoles and quadrupoles toward series production," *IEEE Trans. Appl. Supercond.*, vol. 13, no. 2, pp. 1221–1228, Jun. 2003.

[7] O. Brüning et al., LHC Design Report. Geneva: CERN, 2004. [Online]. Available: https://cds.cern.ch/record/782076

[8] "High-precision resistance Y169025R0000T9L," VISHAY.

[9] P. J. Rousseeuw, "Silhouettes: A graphical aid to the interpretation and validation of cluster analysis," *J. Comput. Appl. Math.*, vol. 20, pp. 53–65, 1987. [Online]. Available: https://www.sciencedirect.com/science/article/pii/0377042787901257

[10] C. M. Bishop, *Pattern Recognition and Machine Learning*. Berlin, Germany: Springer, 2006.

[11] L. Breiman, "Random forests," *Mach. Learn.*, vol. 45, no. 1, pp. 5–32, Oct. 2001, doi: 10.1023/A:1010933404324.

[12] B. Bellesia et al., "Trends in cable magnetization and persistent currents during the production of the main dipoles of the large hadron collider," *IEEE Trans. Appl. Supercond.*, vol. 15, pp. 1213–1216, Jun. 2005.

[13] E. Ravaioli, "Persistent-currents magnetization in STEAM-LEDET," CERN, Geneva, Tech. Rep. EDMS 2418186, 2020.

[14] R. Saederup, "Local transfer function measurement (TFM) data analysis," CERN, Geneva, Tech. Rep. EDMS 2675917, 2021.

[15] E. Ravaioli, "Analytical calculation of the effect of beam-screen eddy currents on the impedance of an lhc main dipole magnet," CERN, Geneva, Tech. Rep. EDMS 2682436, 2022.

[16] N. Kos, "GDOES analyses of 50 and 75 microns OFE copper layer beam screen samples, produced by HEREAUS," CERN, Geneva, Tech. Rep. EDMS 340852 v.1, 2002.

[17] M. Wilson, *Superconducting Magnets*. Oxford, U.K.: Oxford Univ. Press, 1983.

[18] A. P. Verweij, "Electrodynamics of superconducting cables in accelerator magnets," Ph.D. dissertation, Twente U., Twente, 1995, presented on 15 Sep. 1995. [Online]. Available: https://cds.cern.ch/record/292595

[19] C. C. Aggarwal, *Outlier Analysis*. New York, NY, USA: Springer, 2013.

[20] Y. Zhao, Z. Nasrullah, and Z. Li, "Pyod: A python toolbox for scalable outlier detection," *J. Mach. Learn. Res.*, vol. 20, no. 96, pp. 1–7, 2019. [Online]. Available: http://jmlr.org/papers/v20/19-011.html

[21] C. Obermair et al., "Interpretable anomaly detection in the LHC main dipole circuits with non-negative matrix factorization," *IEEE Trans. Appl. Supercond.*, vol. 34, no. 4, Jun. 2024, Art, no. 4004112.